PARAMETRIC STUDY OF A NOVEL GROOVE DESIGN FOR DRY GAS SEALS

Draft Paper

Kefalas A.* Benra F.-K., Brillert D. and Dohmen H. J.
*Author for correspondence
Chair of Turbomachinery,
University of Duisburg-Essen,
Germany,
E-mail: alexander.kefalas@uni-due.de

ABSTRACT

This paper presents a performance analysis of a novel bi-directional groove design for dry gas seals. The scope of analysis includes the impact of important groove design parameters on the dry gas seal performance. The leakage flow and the axial stiffness and damping force coefficients are taken into account for performance assessment. For varying geometry the pressure field in the lubrication gap of the application is estimated. Based on these pressure fields the performance parameters are calculated. The utilized method to predict the fluid flow through the lubrication gap is founded on the Reynolds theory of lubrication. This two dimensional approach is based on the assumptions of a laminar viscous flow field with isothermal conditions and takes aerostatic as well as aerodynamic effects into account. The 2D approach is solved by a finite difference approximation. The aim of the contribution is to recommend geometrical parameters to ensure large static stiffness and damping force coefficients while still allowing for low seal leakage rates.

INTRODUCTION

Applications based on the technology of two non-contacting rotating rings, separated by a thin fluid film, are in the focus of development in various mechanical engineering sectors. The possibility of replacing a common technical application by this novel technology has several advantages. Primarily the opportunity of reducing weight and geometrical properties results in lower power consumption and reduced turbo-machine dimensions, at the same or even improved operation performance. Furthermore, a significant potential of leakage rate reduction is assured through the application.

An established configuration consists of the stationary ring (non-rotating stator) positioned in the casing and the rotating ring (rotor) attached to the shaft of the turbo-machine. The configuration is depicted in Figure 1. In machine downtime the stationary ring, with freedom in axial direction, is shifted against the opposite ring, by an induced closing force (spring). Therefore the application is closed. During operation, the stationary ring lifts off the rotating ring. Owing to aerostatic and aerodynamic forces a fluid film of only a few micrometers develops between the facing surfaces. The originating axial gap between the facing surfaces ranges between 1-10 µm. The application is adaptable to operating pressures applied at the outer ($p_2>p_1$) or the inner diameter ($p_2<p_1$). In both cases a pressure distribution between the two pressure levels develops. To take influence on this pressure distribution one of the facing surfaces contains repetitive grooved sections. By changing the ring's topography, a significant impact on the aerodynamic force is achieved. A high aerodynamic force is essential to build up a fluid film rapidly, especially during the machine startup. Thereby, the duration of friction of the facing surfaces during times of no lubrication or mixed lubrication is reduced. This results in increased lifetime and reduced power losses.

The theoretical analysis of fluid flow in narrow gaps has been a subject of research since the middle of the last century. From the beginning most investigations focus on spiral groove thrust bearings (SGTBs) and spiral groove face seals (SGFSs). Muijderman [1] presents the Narrow Groove Theory (NGT) for analysis of flat, spherical and conical SGTBs and approximate formulations are given for pressure, resulting loads, friction torque, and the coefficient of friction. A limited number of experiments are also reported for SGTBs and comparisons with the given analyses are favorable for incompressible fluids. Limitations of the NGT are apparent and extensions to the original analyses appear to account for more realistic configurations. Considering both SGFS and Rayleigh step seals, Cheng, et al. [2] discuss the relative placement of grooves and seal dams in a NGT analysis for compressible fluids. Seal dams on the low pressure side of a SGFS minimize leakage rate at the expense of axial stiffness at low speeds. For these lower speeds, seal dams on the high pressure side give higher values of stiffness. Considering a flat, spherical, conical and cylindrical groove geometry, Smalley [3] describes the NGT in generalized coordinates and solves the governing equations with finite differences to give load, capacity, power loss, leakage rate and stiffness coefficients.

Experimental studies in addition to that presented by Muijderman include those studies reported by James and Potter [4] on ceramic SGTBs. Static loads with 10 percent possible error and an optimum bearing geometry are verified from the experiments. DiRusso [5][6] presents measurements of film thickness and drag torque for various SGFS configurations.

The analysis of compressible fluid grooved seals at varying compressibility number (Λ) is difficult due to the non-linearity of the Reynolds equation which results in steep pressure gradients near the groove to dam interfaces. Numerical methods often have difficulties in convergence, thus requiring fine meshes to ensure reliable solutions. Furthermore, the effect of

frequency excitations on the dynamic force performance of SGFSs is largely ignored. Hunger [7] and Zirkelback et al. [8] describe this effect using numerical approaches.

The authors' intent is to extend performance analyses of applications based on the technology of two non-contacting rotating rings. Therefore performance analysis of a dry gas seal (DGS) with a novel groove design is executed. A Finite Difference Method (FDM) analysis of isothermal, compressible fluid follows. Perturbations of the non-linear Reynolds equation determine differential equations from which the dynamic axial force coefficients result. The static and dynamic force performance of the novel designed DGS is analyzed as a function of various geometrical parameters.

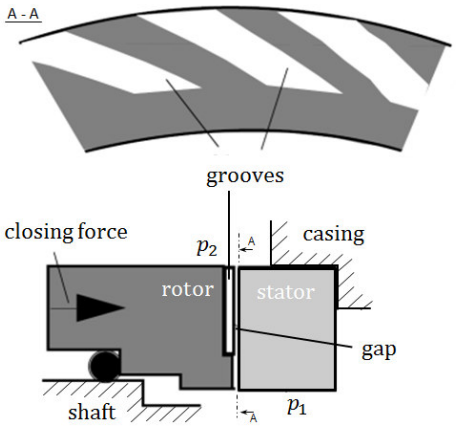

Figure 1 Arrangement of rotor and stator

NOMENCLATURE

C_z	[N·s/m]	Axial damping coefficient
$C_{z,dim}$	[-]	Dimensionless axial damping coefficient: C_z/C_{z*}
F	[N]	Force
H	[-]	Normalized fluid film depth
h	[m]	Fluid film depth
l_g	[-]	Groove extend: $(\Delta r_g)/\Delta r$
K_z	[N/m]	Axial stiffness coefficient
$K_{z,dim}$	[-]	Dimensionless axial stiffness coefficient: K_z/K_{z*}
n	[-]	Iteration step
n_g	[-]	Number of grooves
P	[-]	Normalized pressure
p	[Pa]	Pressure
Q	[g/s]	Leakage rate
Q_{dim}	[-]	Dimensionless Leakage rate: Q/Q_*
R	[-]	Normalized radius
r	[m]	Radius
T	[K]	Temperature
t_k	[m]	Maximal fluid film depth in groove
t	[s]	Time
U	[1/s]	Rotational speed
w	[m]	width
Z	[N/m]	Complex impedance

Special characters

β	[deg]	Section angle
ε_0	[-]	Convergence accuracy
γ_{d_r}	[-]	Groove depth ratio: $t_k/\Delta r \cdot e03$
$\gamma_{w\ r}$	[-]	Groove width ratio: $w_g/(w_g+w_l)$
Λ	[-]	Compressibility number (bearing number)
η	[Pa·s]	viscosity of fluid
Θ	[-]	Normalized circumferential direction
θ	[deg]	Circumferential direction
ρ	[kg/m^3]	Density
ω	[rad/s]	Angular velocity
ω_{ex}	[1/s]	Frequency of dynamic axial motions
σ	[m]	Surface roughness

Subscripts

dim	dimensionless
g	groove
i	inner
l	land
m	mean
max	maximum
min	minimum
o	outer
rat	ratio
ref	reference
*	Performance result based on initial seal geometry

GOVERNING EQUATION OF 2D APPROACH

The basic equation for calculating the pressure of a compressible fluid in the sealing gap is based on the *Reynolds theory of lubrication*. This theory is derived from the Navier-Stokes equations of motion and the condition of continuity of the fluid based on certain assumptions.

Assumptions

Based on the *Reynolds theory of lubrication* the following assumptions are defined:

- Ideal gas behavior
- Isothermal and isoviscous conditions
- Laminar flow
- Smooth seal faces
- No misalignment of facing surfaces
- Rigid faces

Unless detailed examination of the gas properties is not required, the fluid is of Newtonian nature and ideal gas behavior is accepted in narrow gap analyses. Since moderate rotational speed and low pressure conditions are subjects in the present analysis, laminar flow is defined. Additionally, it is assumed that no turbulence or vortices develop in the flow. Non-contact of the facing seal faces is defined. Therefore, heat generation is very small and the temperature gradient is negligible. The gas viscosity is relatively insensitive to pressure and temperature variation. Based on this fact, isoviscosity is stated. In the present study, fluid flow at full lift-off is examined. Therefore, effects on the flow due to surface roughness are ignored. These effects are merely significant in the mixed lubrication regime. In case of mixed lubrication, the surface roughness of the facing surfaces (σ) equals the fluid film thickness (h_{min}) in between the facing surfaces [9][10]. Patir and Cheng [11][12] stated that surface roughness is

significant mostly in regimes where h/σ≤3 is valid. By reasons of accurate manufacturing of facing surfaces (lapping) and face material choice σ typically exhibits a value about 0.1 µm [10][13]. Therefore, smooth seal faces are defined. Figure 2 illustrates the determined fluid body parameters in between the parallel facing surfaces of stator and rotor for a repetitive ring section. In between the parallel facing surfaces, the fluid film thickness is marginal compared to other dimensions of length. Therefore, the velocity gradients in circumferential and radial direction are the significant and hence determining velocity gradients. Viscosity, pressure and temperature are presumed to be constant across the fluid body thickness.

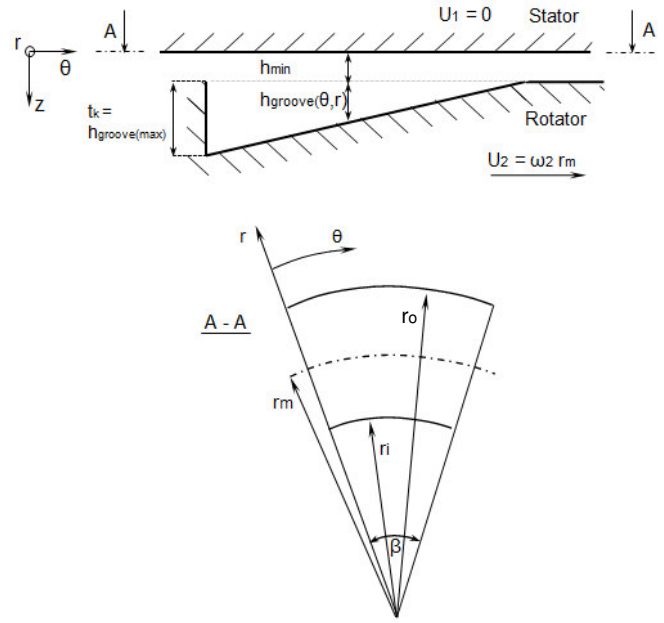

Figure 2 Sealing gap parameters

NUMERICAL METHOD

The Reynolds equation in cylindrical coordinates for an isoviscous, ideal gas ($\rho=p/R_s \cdot T$) under laminar and isothermal flow conditions within the facing seal faces is

$$\frac{1}{r}\frac{\partial}{\partial\theta}\left(ph^3\frac{\partial p}{\partial\theta}\right)+r\frac{\partial}{\partial r}\left(ph^3\frac{\partial p}{\partial r}\right)=6\eta\omega r\frac{\partial(ph)}{\partial\theta}+\frac{\partial(ph)}{\partial t}\,. \qquad (1)$$

Using the definitions

$$R=\frac{r}{r_m},\ \Theta=\frac{\theta}{r_m},\ P=\frac{p}{p_{ref}},\ H=\frac{h}{t_k},\ \Lambda=6\eta\omega\frac{{r_m}^2}{p_{ref}t_k^2}$$

equation (1) can be transformed into the normalized form:

$$\frac{1}{R}\frac{\partial}{\partial\Theta}\left(PH^3\frac{\partial P}{\partial\Theta}\right)+R\frac{\partial}{\partial R}\left(PH^3\frac{\partial P}{\partial R}\right)=\Lambda\frac{\partial(PH)}{\partial\Theta}\,. \qquad (2)$$

Equation (2) is the basic equation for the *Reynolds theory of lubrication* to describe the time-independent fluid flow in between two parallel surfaces of different relative movements. It is the governing equation for the chosen 2D-method to determine the pressure distribution in the sealing gap. The normalized fluid film depth (H) equals to ($H_{min}+H_g$) in the groove and (H_{min}) in the land and dam regions. Λ represents the compressibility number, commonly known as bearing number. Normalized pressures at the inner and outer radius are specified as

$$\mathrm{P}(R_i,\Theta)=P_i\ ,\ \mathrm{P}(R_o,\Theta)=P_o, \qquad (3)$$

and, since circumferential thermal distortion and misalignments of the faces are not taken into account, the circumferential pressure distribution for each repeating groove and land section is periodic:

$$\mathrm{P}(R,\Theta_0)=P\left(R,\Theta_{2\pi/ng}\right) \qquad (4)$$

A successive approximation scheme based on the Newton-Raphson method is adopted for the iterative solution of equation (2). The FDM is used to discretize the equation. The established 2D calculation grid is formulated by a general matrix K_{MN}. This nonsymmetrical matrix is banded by the non-zero terms at the upper right and lower left corners, due to boundary conditions and the grid numbering algorithm. Only the terms within the bandwidth are stored. The general nonsymmetrical banded matrix is first factored into upper and lower triangular matrices. The solution can then be calculated by a back-substitution scheme. At each iteration, the matrix K_{MN} is updated. The convergence condition is defined by:

$$\varepsilon=\frac{\left|P^{n+1}-P^n\right|}{\left|P^n\right|}\leq\ \varepsilon_0 \qquad (5)$$

where P^n are the dimensionless pressure values at iterative step n; P^{n+1} are those at step n+1 and ε_0 is the convergence accuracy defined as $1.0\text{x}10^{-6}$. A more detailed description of the presented numerical model is described in Kefalas et al. [14].

To determine the seal stiffness and damping force coefficients, the rotating surface is considered to undergo small axial motions (Δz) relative to an equilibrium position (h_o) at an excitation frequency (ω_{ex}). The fluid film depth is equal to

$$\mathrm{h}(\mathrm{r},\Theta,\mathrm{t})=h_o(r,\Theta)+\Delta z e^{i\omega_{ex}t};i=\sqrt{-1} \qquad (6)$$

The resulting pressure is also described by the superposition of zeroth- and first-order pressure fields,

$$\mathrm{p}(\mathrm{r},\Theta,\mathrm{t})=p_o(r,\Theta)+p_1(r,\Theta)\Delta z e^{i\omega_{ex}t} \qquad (7)$$

Substitution of the equilibrium and the perturbed fluid film depth and pressure into the Reynolds equation results in equation (1) for (p_0, h_0) and the first-order equation for (p_1) as

$$\frac{1}{r}\frac{\partial}{\partial\theta}(\dot{m}_{r1})+r\frac{\partial}{\partial r}(\dot{m}_{\theta 1})+i\omega_{ex}(p_1h_0+p_0)=0 \qquad (8)$$

where the first-order radial and circumferential mass flow rates are

$$\dot{m}_{r1} = -\frac{1}{12\eta}\left(3{h_0}^2 p_0 \frac{\partial p_0}{\partial r} + {h_0}^3 \frac{\partial (p_0 p_1)}{\partial r}\right) \tag{9}$$

$$\dot{m}_{\theta 1} = -\frac{1}{12\eta}\left(3{h_0}^2 p_0 \frac{\partial p_0}{\partial \Theta} + {h_0}^3 \frac{\partial (p_0 p_1)}{\partial \Theta}\right) + \frac{\omega r}{2}(p_0 + h_0 p_1) \tag{10}$$

Integration of the first-order field (p_1) on the seal surface gives stiffness (real part) and damping (imaginary part) coefficients, together representing a complex impedance

$$Z = K_z + i\omega_{ex} C_z = -n_g \int_{r_i}^{r_o} \int_{o}^{\beta} p_1(r,\theta) r d\theta dr \tag{11}$$

In dependence on equation (1), equation (8) is transferred into the normalized form, based on the same definitions, and discretized by a FDM method. The same successive approximation scheme is used to solve the resulting set of equations.

RESULTS AND DISCUSSION

A parametric study for the dry gas seal with a novel groove design helps to ascertain the seal geometry for best static and dynamic seal behavior. The basic geometry is shown in figures 3a-c and its variation for the present parametric study is given in table 1. The initial groove geometry represents a narrow width seal ratio ($R_{rat}=r_o/r_i=1.27$) with twenty grooves and a groove extend of $l_g=0.74$. The pressure ratio ($P_{rat}=p_o/p_i=20$) represents a large pressure drop across a typical gas face seal. The nominal parameters are set to the published values, i.e. groove width ratio $\gamma_{w\_r}=0.65$ and groove depth ratio $\gamma_{d\_r}=0.72$. Based on this initial seal geometry the reference performance result (Q_*, K_{z*}, C_{z*}) are determined to state the dimensionless performance parameters in figures 4-11.

Effect of the Number of Grooves (n_g)

The dimensionless leakage rate remains unchanged with increasing groove number (n_g) after increasing prominently from $n_g=5$ to $n_g=15$ (Fig. 4). In general, the leakage rate depends on the fluid film depth in the groove region ($h_{min}+h_g$). With increasing groove number the groove clearance increases, but the minimum fluid film depth (h_{min}) of the force equilibrium situation ($F_o/F_c\sim1$) does not change significantly for a high amount of grooves. Therefore, strong changes in leakage rate are solely depicted for $n_g<15$. The dimensionless axial stiffness coefficient ($K_{z,dim}$) rises from the smallest value of n_g and reaches an asymptotic value, as the number of grooves becomes larger (Fig. 5). The dimensionless axial damping coefficient ($C_{z,dim}$) reaches a minimum at $n_g=20$, before rising slightly for increasing groove numbers (in dependence on $K_{z,dim}$). Based on these results, a surface topography arrangement with 18

Table 1 Parametric variation of groove design

Variation	n_g	$\gamma_{w\_r}=w_g/(w_g+w_l)$	$l_g=(\Delta r_g)/\Delta r$	$\gamma_{d\_r}=t_k/\Delta r \cdot e03$
Number of grooves (n_g)	5-30	0.65	0.74	0.6
Groove width ratio γ_{w_r}	20	0.32 - 0.79	0.74	0.6
Groove extend l_g	20	0.65	0.5 – 0.9	0.6
Groove depth ratio γ_{d_r}	20	0.65	0.74	0.16 – 0.96
compressibility number (Λ)=98; Fluid Properties: η=1.9·10-5 Pa·s, R_s=287.058 J/(kg·K), T=333.15 K				

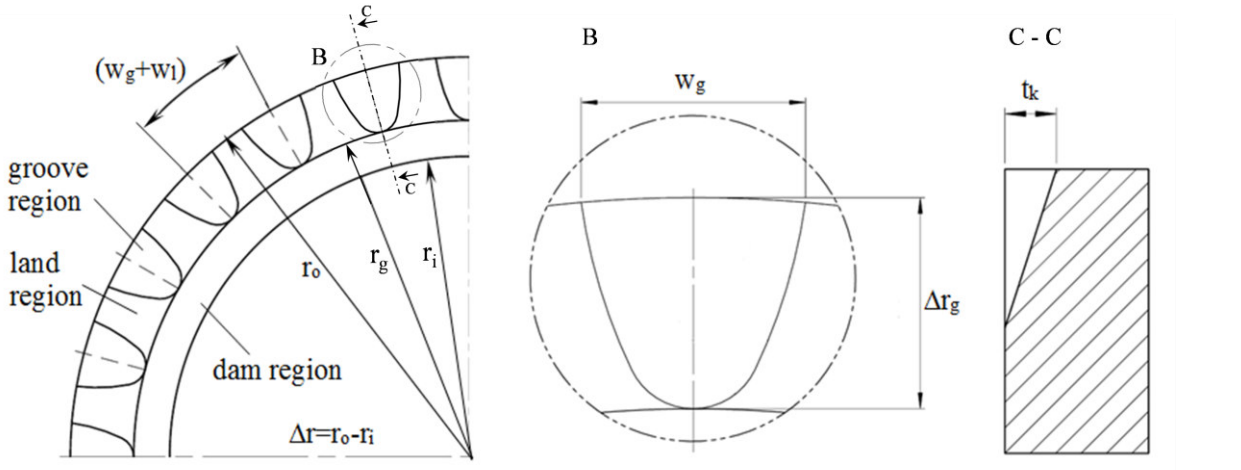

a – Arrangement of grooves on ring surface b – Design of novel groove c – Cross-section of grooved ring

Figure 3 Groove geometry and arrangement on ring-surface

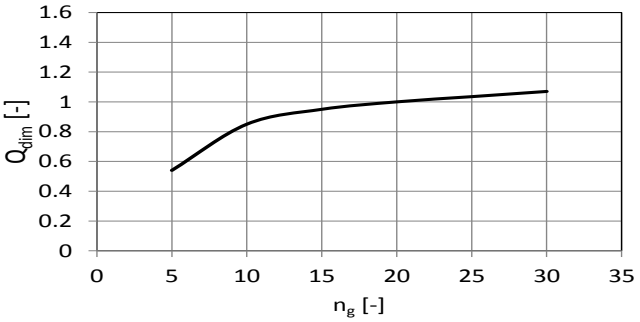

Figure 4 Variation of dimensionless leakage rate with the number of grooves (n_g)

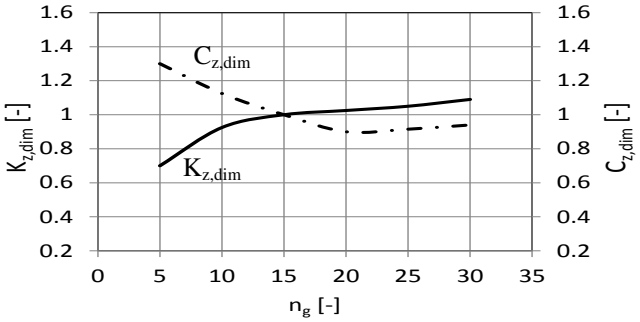

Figure 5 Variation of dimensionless force coefficients with the number of grooves (n_g)

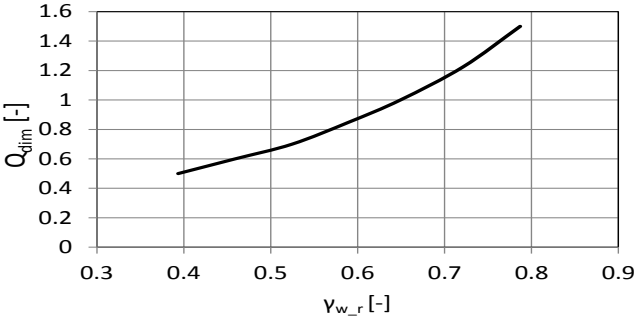

Figure 6 Variation of dimensionless leakage rate with the groove width ratio (γ_{w_r})

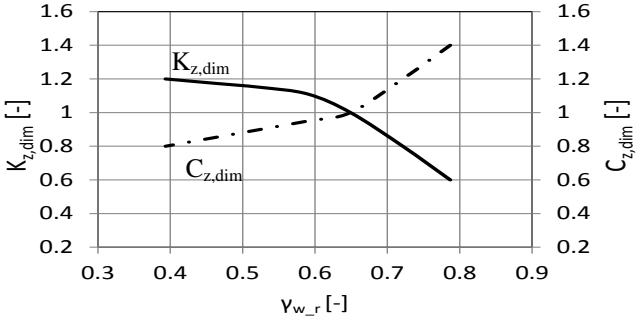

Figure 7 Variation of dimensionless force coefficients with the groove width ratio (γ_{w_r})

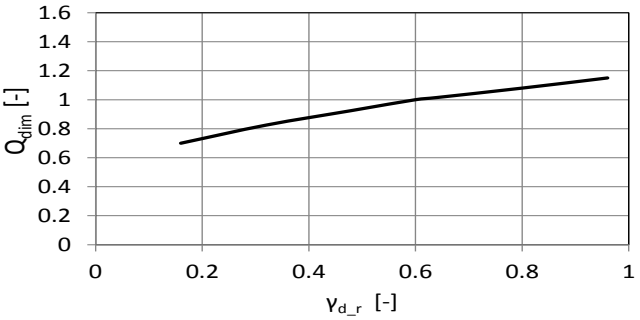

Figure 8 Variation of dimensionless leakage rate with the groove depth ratio (γ_{d_r})

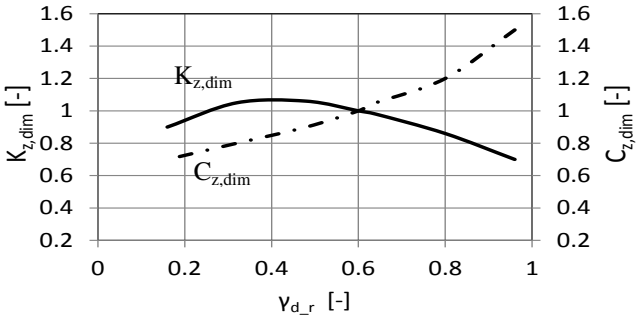

Figure 9 Variation of dimensionless force coefficients with the groove depth ratio (γ_{d_r})

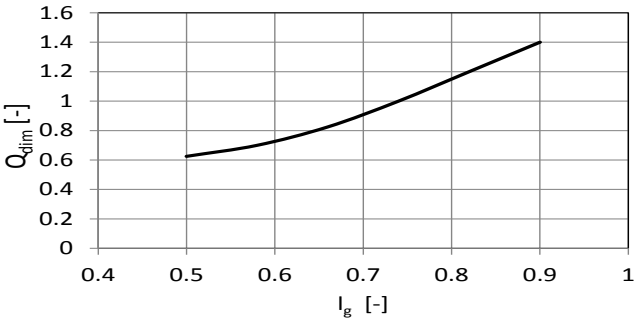

Figure 10 Variation of dimensionless leakage rate with the groove extend (l_g)

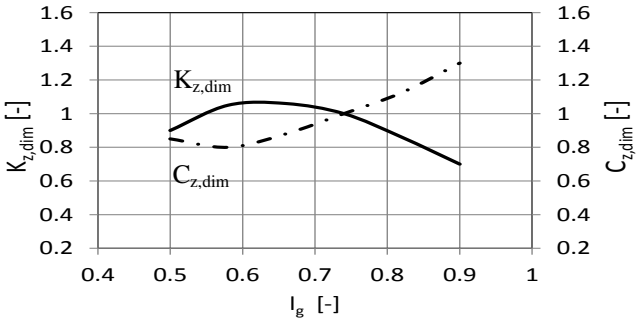

Figure 11 Variation of dimensionless force coefficients with the groove extend (l_g)

grooves should be chosen, since this number ensures operation with relatively high stiffness and damping coefficients.

Effect of the Groove Width Ratio (γ_{w_r})

An increasing groove width ratio results in an increase of the dimensionless leakage rate. The impact of this ratio on the leakage rate is high (Fig. 6), compared to the influence of i. e. the groove number or groove depth ratio. The dimensionless stiffness coefficient decreases slightly with increasing groove width ratios up to γ_{w_r}=0.6. Passing this value the stiffness coefficient decreases strongly. Regarding the dimensionless damping coefficient the depicted characteristic reverses. As the stiffness coefficient shows nearly constant values for γ_{w_r}<0.6 and to ensure a high damping coefficient, a groove width ratio of γ_{w_r}=0.6 is recommended.

Effect of the Groove Depth Ratio (γ_{d_r})

Figure 8 indicates a rise of the dimensionless leakage rate as the groove depth ratio increases. This is based on the increasing fluid film depth in the groove region (h_{min}+h_g) with increasing groove depth. For γ_{d_r}>0.6 the magnitude of increase of leakage rate decreases slightly as the impact of groove depth on the average seal clearance reduces. The dimensionless stiffness coefficient increases for γ_{d_r}<0.48 and decreases prominently for γ_{d_r}>0.48. Aiming for the highest stiffness coefficient for designing the surface topography, the maximum value γ_{d_r}=0.48 determines the optimum groove depth value (Fig. 9). In contrast to the stiffness coefficient, the dimensionless damping coefficient increases as the groove depth ration increases.

Effect of the Groove Extend (l_g)

Figure 10 shows that the leakage rate increases with increasing groove extend (l_g). This is based on the average clearance of the face seal, which also increases as the groove region covers more of the seal face area. In dependence on the groove depth ratio (γ_{d_r}), the dimensionless stiffness coefficient increases for small values of the groove extend (l_g<0.66) and decreases with increasing groove region extend in radial direction (Fig. 11). In contrast to the results of γ_{d_r} variation, the dimensionless damping coefficient values do not show a continuous increase. A minimum damping coefficient is calculated for l_g=0.58. Based on these results, a groove extend of l_g=0.7 should be chosen, since this extend ensures operation with nearly the highest stiffness coefficient and a relative high damping coefficient at same time.

CONCLUSION

A finite difference analysis for isothermal, compressible fluid flow through a dry gas seal with a novel groove design has been detailed along with a successive approximation scheme based on the Newton-Raphson method for the iterative solution of the nonlinear Reynolds equation. Zeroth- and first-order pressure fields are calculated for the force equilibrium situation. The leakage rate and the force coefficients (stiffness and damping) are predicted for varying parameters of the groove design. Based on the calculation of the dry gas seal performance characteristics as the seal geometry changes, the optimum geometry for the novel groove design is identified by: number of grooves (n_g) =18, groove width ratio (γ_{w_r}) =0.6, groove depth ratio (γ_{d_r}) =0.48 and groove extend (l_g) =0.7.

The parametric study executed to analyse the DGS behaviour with the novel groove design yields interesting results for operation performance. The results show that the number of grooves (n_g>15) and the groove depth have small impact on the leakage flow. The leakage rate is strongly influenced by changes in groove extend and width. Regarding the groove extend and the groove depth only a certain geometrical configuration ensures a high axial stiffness coefficient ($\bar{K}_z$). The number of grooves (n_g>15) and the groove width (γ_{w_r}<0.6) allow a nearly constant characteristic. Aside from the constant range a selection of geometrical setting is not recommended as changes in n_g and γ_{w_r} result in high losses of axial stiffness. The determined axial damping coefficient ($C_{z,dim}$) depicts identical characteristics for the parameter of groove extend, groove depth and width. With increasing value of these parameters the axial damping coefficient increases. Regarding groove depth and extend $C_{z,dim}$ is not the determining performance parameter, as dry gas seals are traditionally designed featuring high axial stiffness. In case of the number of grooves and groove width $C_{z,dim}$ is included into the seal design decision as $K_{z,dim}$ depicts a nearly constant range for varying design parameters. In this particular case aiming for high axial damping is the premise. Content of prospective investigation is the performance comparison of a dry gas seal with the novel groove design and other utilized groove designs.

REFERENCES

[1] Muijderman, E. A., “Spiral groove bearings”, Thesis, Technological University Delft, 1964, pp. 24-58.

[2] Cheng, H. S., Castelli, V. and Chow, C. Y., “Performance Characteristics of Spiral-Groove and Shrouded Rayleigh Step Profiles for High-Speed Noncontacting Gas Seals” , ASME Journal of Lubrication, 91, pp. 60-68, 1970

[3] Smalley, A. J.,”The Narrow Groove Theory of Spiral Groove Gas Bearings: Development and Application of a Generalized Formulation for Numerical Solution”, ASME Journal of Lubrication, 92, pp 495-503, 1969

[4] James, D. D. and Potter, A. F., ”Numerical Analysis of the Gas-Lubricated Spiral-Groove Thrust Bearing-Compressor”, ASME Journal of Lubrication, 89, pp. 439-444, 1967.

[5] DiRusso, E., “Film Thickness Measurement for Spiral Groove and Rayleigh Step Lift Pad Self-Acting Face Seals.” NASA Technical Paper 2058, 1982.

[6] DiRusso, E., ”Dynamic behavior of spiral-groove and Rayleigh-step self-acting face seals” NASA Technical Paper 2266, 1984.

[7] Hunger, H., “Calculation of static and dynamic characteristics of aerodynamic journal bearings” Diss., University of Karlsruhe, 1982

[8] Zirkelback, N., “Finite Element Analysis of Herringbone Grooved Journal Bearings: A Parametric Study”, ASME Journal of Tribology, 120, pp. 234-240,

1998.
[9] Constantinescu, V. N., “Gas lubrication”, The American Society of mechanical engineers, pp. 48-90, 1969
[10] Lebeck, A. O., “Principles and design of mechanical seals”, pp. 107-132, 1991
[11] Patir, N. Cheng, H.S., "An average flow model for determining effects of three dimensional roughness on partial hydrodynamic lubrication", Journal of Lubrication,100, pp. 12-17, 1978
[12] Patir, N., Cheng, H. S., "Application of average flow model to lubrication between rough sliding surfaces." Journal of Lubrication, 101, pp. 220-230, 1978
[13] Szeri, A. Z., “Fluid film lubrication”, Cambridge University Press, 2011
[14] Kefalas, A., Benra, F. K., Dohmen, H.J., “Numerical analysis of compressible fluid flow in narrow gaps”, FEDSM 2014-21128, 2014